

# Structure of Multicomponent Coulomb Crystals

M. E. Caplan\*

*Illinois State University, Normal, IL 61761 USA*

(Dated: November 14, 2019)

Coulomb plasmas crystallize in a number of physical systems, such as dusty plasmas, neutron star crusts, and white dwarf cores. The crystal structure of the one component and binary plasma has received significant attention in the literature, though the less studied multicomponent plasma may be most relevant for many physical systems which contain a large range of particle charges. We report on molecular dynamics simulations of multicomponent plasmas near the melting temperature with mixtures taken to be realistic X-ray burst ash compositions. We quantify the structure of the crystal with the bond order parameters and radial distribution function. Consistent with past work, low charge particles form interstitial defects and we argue that they are in a quasi-liquid state within the lattice. The lattice shows screening effects which preserves long range order despite the large variance in particle charges, which may impact transport properties relevant to astrophysics.

## I. INTRODUCTION

Coulomb (Yukawa) plasmas consist of a set of charged point particles interacting via a Coulomb repulsion which is screened by a neutralizing background gas. At sufficiently high pressure (or density) these systems can crystallize even despite astronomically high temperatures.

The properties of these ‘astromaterials,’ materials present in stars, impact observations relevant to a number of astrophysical phenomena. To name a few, (1) latent heat release in freezing white dwarfs is now observed to affect the cooling of white dwarfs [1], (2) phase separation of heavy nuclei in the oceans of freezing white dwarfs may release additional gravitational potential energy which affects cooling [1, 2], and (3) the thermal transport properties of the phase separated neutron star crust in accreting X-ray binaries must be known to interpret observations of X-ray binaries in quiescence [3–5].

The one-component plasma (OCP) is now well studied and is known to undergo a first order phase transition between a liquid and solid phase [4, 6, 7]. Phase separation and diffusion of the binary mixture has also received attention in the literature [8–10]. Analytic models of ternary mixtures have been used to approximate the phase separation of mixtures with many components near their eutectic point [3]. Past work studying the structure of a few specific multicomponent plasma (MCP) mixtures found that they tended to form a bcc lattice with a number of complicated compositionally driven defects. [3, 11–15].

Electron scattering in MCPs is relevant for astrophysics, as electron-impurity scattering affects the thermal and electrical conductivity (see for example Brown and Cumming 5). Astrophysical models use the impurity parameter,  $Q_{imp} = (1/n)\sum_i n_i (\bar{Z} - Z_i)^2$  (defined as the variance in mixture charge), to calculate mixture transport properties. However, the impurity parameter formalism may overpredict the electron scattering frequency

by assuming a random distribution of impurities [16, 17]. While this assumption may be valid for nearly pure mixtures with trace impurities, mixtures with many components may have more complicated lattice structures which may not necessarily enhance the electron scattering rate as much as a random impurity distribution might predict. For example, consider a binary ionic mixture (BIM) studied by Ogata *et al.* 16. A BIM with equal abundances of species  $Z_1$  and  $Z_2$  may have a ground state CsCl-structure, with each ion of species 1 being at the center of a cube of eight ions of species 2 and vice versa. With this long range order such a crystal would effectively have no defects, though a large  $Z_1/Z_2$  would yield a high  $Q_{imp}$  suggesting otherwise.

Simulations studying specific MCPs are thus well motivated astrophysically. In past work, Horowitz *et al.* studied the phase separation of one mixture and calculated the static structure factor  $S(q)$  of the resulting solid to determine the thermal transport properties [14, 15]. Roggero and Reddy 18 have recently used a Path Integral Monte Carlo approach to determine the electron scattering rate in multicomponent plasmas and find that the effective lattice impurity is reduced by a factor of a few relative to theoretical calculations using the impurity parameter. In contrast, having a large number of species may introduce many new kinds of disorder (relative to the OCP) even if the lattice structure is regular as in the BIM case considered above. Trace low  $Z$  impurities have been observed to form clusters of interstitial defects, suggesting they separate and form pockets of disorder within the lattice [3, 15]. Furthermore, phase separation may produce crystalline domains which are locally purified in order to accommodate the entire mixture. Grain boundaries between such ‘compositional domains’ could act as sites for electron scattering which may be important depending on their size [3].

In this work we study the structure of six crystalline MCPs produced from molecular dynamics (MD) simulations using the bond order parameter and radial distribution functions. In Sec. II we discuss our formalism, including our MD code (Sec II A), our methods of calculating the bond order parameter and radial distribution

---

\* mecapl1@ilstu.edu

functions (Secs. IIB and IIC), and a brief discussion of the theory of OCPs and MCPs (Sec. IID). We describe our simulations and results in Sec. III and conclude in Sec. IV.

## II. FORMALISM

### A. Molecular Dynamics

Nuclei in Coulomb plasmas are fully ionized and are treated as point particles (ions) which interact via a two-body screened Coulomb potential

$$V(r_{ij}) = \frac{Z_i Z_j e^2}{r_{ij}} \exp(-r_{ij}/\lambda), \quad (1)$$

where  $Z_i$  and  $Z_j$  are the electric charges of the  $i^{\text{th}}$  and  $j^{\text{th}}$  nuclei and  $r_{ij}$  is the separation between them. The exponential term is due to the screening from the degenerate electron gas between ions and is calculated using the Thomas Fermi screening length  $\lambda^{-1} = 2\alpha^{1/2}k_F/\pi^{1/2}$  using the fine structure constant  $\alpha$  and electron Fermi momentum  $k_F = (3\pi^2 n_e)^{1/3}$ . For the MCP we require the electron density  $n_e$  to be equal to the charge density from the ions (*i.e.*  $n_e = \langle Z \rangle n$  with ion number density  $n$  and average charge  $\langle Z \rangle$ ). Electrons are not included explicitly; their effects on the lattice are included through the potential screening.

To evolve the system we solve Newton's equations of motion numerically using a velocity Verlet scheme with the Indiana University Molecular Dynamics (IUMD) CUDA-Fortran code, version 6.3.1. This code has been used extensively to study astromaterials in neutron star crusts and white dwarfs and is described in more detail in past work [3, 11, 15]. All simulations presented in this work use periodic boundary conditions and cubic simulation volumes.

### B. Bond Order Parameter

We quantify the local order of the lattice around nuclei of each species in our simulations with the bond order parameter  $Q_6$ . This allows us to evaluate the 'solidness' or 'liquidness' of each nucleus with a simple metric determined from the relative positions of its nearest neighbors. For an individual ion,  $Q_6$  generally takes on a value between 0 and 0.5. Past work by Lechner and Dellago 19 have shown that in Lennard-Jones mixtures at finite temperatures one expects  $Q_6 \sim 0.44$  in a bcc lattice, which is similar to what was reported by Caplan *et al.* 3 when studying phase separation in Coulomb crystals.

We calculate  $Q_6$  (as in Wang *et al.* 20) by

$$Q_6 = \sqrt{\frac{4\pi}{13} \sum_{m=-6}^6 \left| \frac{1}{N_b} \sum_{\text{bonds}} Y_{6m}(\theta(\mathbf{r}), \phi(\mathbf{r})) \right|^2} \quad (2)$$

for each particle. Spherical harmonics  $Y_{6m}$  are calculated from the angles  $\theta(\mathbf{r})$  and  $\phi(\mathbf{r})$  of the vector between pairs of nuclei. This is averaged over nearest neighbors and harmonics to produce the coordinate independent  $Q_6$ .

### C. Radial Distribution Function

We calculate the radial distribution function  $g(r)$  for ions in our mixtures. As mixtures contain many species, we must consider the radial distribution functions between species  $g_{ij}(r)$ , following the definition used by Thorneywork *et al.* 21,

$$c_i c_j g_{ij}(r) = \frac{1}{N\rho} \left\langle \sum_{\mu=1}^{N_i} \sum_{\nu \neq \mu}^{N_j} \delta(\mathbf{r} + \mathbf{r}_\mu - \mathbf{r}_\nu) \right\rangle \quad (3)$$

where  $c_{i,j}$  are the concentrations of the  $i^{\text{th}}$  and  $j^{\text{th}}$  species,  $N$  is the total number of particles in the mixture,  $\rho$  is the total number density, and the sums are over all pairs of particles of species  $i$  and  $j$ . Distances  $\mathbf{r}_\mu - \mathbf{r}_\nu$  are taken over the periodic boundary. For an OCP we recover the radial distribution function for  $i = j$ . For simplicity and due to the large number of species in our mixtures we will only consider  $i$  as the most abundant species in the mixture (for all of our mixtures  $c_i \gtrsim 0.25$ ). Our normalizations are such that  $g_{ij}(r) = 1$  as  $r \rightarrow \infty$ .

### D. Coulomb Plasmas

#### 1. One-component Plasmas

We discuss one-component plasmas as they will be used for reference when studying mixtures. The one component plasma is characterized by the Coulomb plasma parameter  $\Gamma$ , calculated as

$$\Gamma_{OCP} = \frac{e^2 Z^2}{aT} \quad (4)$$

with squared elementary charge  $e^2$  ( $\approx 1.44$  MeV fm), ion charge  $Z$ , Wigner-Seitz radius  $a = (4\pi n/3)^{-1/3}$  with  $n$  ion number density as before, and temperature  $T$  (in MeV). The critical  $\Gamma_{crit} = 175$  occurs at the melting temperature. It is often useful to report  $\Gamma_{crit}/\Gamma$ , which is linear with temperature and is unity at the melting temperature. When  $\Gamma_{crit}/\Gamma < 1$ , the OCP can form a bcc or fcc lattice, though the bcc lattice is typically the relevant case for neutron stars [4, 6].

#### 2. Multi-component Plasmas

In a mixture, each component of charge  $Z_i$  and concentration  $c_i$  can be characterized individually by  $\Gamma_i =$

$e^2 Z_i^2 / a_i T$  where  $a_i$  must now be defined in terms of the average charge density of the mixture  $\rho_{ch}$ ,  $a_i = (3Z_i / 4\pi\rho_{ch})^{1/3}$ . Averaging over all components gives

$$\Gamma_{MCP} = \frac{\langle Z^{5/3} \rangle e^2}{T} \left[ \frac{4\pi\rho_{ch}}{3} \right]^{1/3}. \quad (5)$$

Observe that a MCP with a high  $\Gamma_{MCP}$  (*i.e.* solid) can have components of low charge, such that  $\Gamma_i < 175$  is possible. It is these ‘liquid-like’ ions present in mixtures, and their effect on the crystal structure of the MCP, that we seek to study. As low  $Z_i$  nuclei have previously been identified as interstitial defects by inspection in simulations by Horowitz *et al.* we are motivated to quantify the degree of ‘liquidness’ of these light nuclei in this work.

### III. SIMULATIONS

#### A. One-component Simulations

We perform simulations of 16,000 ions ( $20 \times 20 \times 20$  bcc unit cells) in a cubic simulation volume with periodic boundary conditions at  $\Gamma_{crit}/\Gamma = 0.25, 0.50, 0.66, 0.97, 1.00, 1.03, 1.33, 1.50, 2,$  and  $4$ . Simulations  $\Gamma_{crit}/\Gamma > 1$  are liquid, while  $\Gamma_{crit}/\Gamma < 1$  are solid. Initial conditions for the liquid were taken to be random ion positions in the simulation volume, while the solid was taken to be a bcc lattice whose planes are aligned with the simulation boundaries. Visualizations are shown in Fig. 1.

For  $\Gamma_{crit}/\Gamma = 1$  we run two simulations, one using random initial conditions and one using lattice initial conditions. At the critical temperature both solid and liquid phases can exist allowing a useful temperature-independent comparison of solid-like and liquid-like behavior. All simulations are run at constant temperature for  $10^6$  MD timesteps with temperature renormalizations every 100 timesteps following the procedure described in Caplan *et al.* All simulations are run using a timestep of 100 fm/c, and an ion density of  $7.18 \times 10^{-5} \text{ fm}^{-3}$ . [22] The total energy converges within the first few thousand timesteps for all simulations, with fluctuations of order  $10^{-5} E_{tot}$ , indicating that configurations quickly reach thermal equilibrium. Total energy remained approximately constant with fluctuations of order  $\Delta E/E \sim 10^{-6}$  during the equilibrium phase.

We calculate the bond order parameter  $Q_6$  for each ion in the final configurations of these simulations, shown in Fig. 2 and Fig. 3. We calculate the local bond order parameter to ions within 35 fm, which corresponds to the first minima in the radial distribution function (Fig. 4) and thus contains the fourteen nearest neighbors (*i.e.* each ion is at the center of a bcc unit cell of eight nuclei, with six nuclei at the center of each adjacent cell).

In Fig. 2 and 3, for  $\Gamma_{crit}/\Gamma \geq 1$ , we observe that the bond order parameter  $Q_6$  forms an approximately Gaussian distribution with a mean near  $Q_6 \approx 0.2$ . This

is expected for a liquid with minimal local order. For  $\Gamma_{crit}/\Gamma \leq 1$ , we observe a strong  $\Gamma$  dependence in the distribution mean and width. For  $\Gamma_{crit}/\Gamma \lesssim 1$ , the distribution shifts quickly toward  $Q_6 \approx 0.4$  as  $\Gamma_{crit}/\Gamma$  decreases. As  $\Gamma_{crit}/\Gamma$  approaches zero the distribution becomes strongly peaked around  $Q_6 \approx 0.5$ . Notably, a gap is observed near  $Q_6 \approx 0.3$ . This region of the histogram is largely unpopulated except for by the tails of a few distributions which are near the critical temperature. This strong separation in  $Q_6$  for the OCP suggests that  $Q_6$  will be a useful tool for discriminating between the solidness and liquidness of ions in MCPs. This technique for discriminating between solid and liquid ions has previously been used in studies of MCP phase separation by Caplan *et al.* 3, though this method was not rigorously developed in that work. The radial distribution function  $g(r)$  shows the known results for bcc solids at low  $\Gamma_{crit}/\Gamma$  and liquids at high  $\Gamma_{crit}/\Gamma$ . The first order phase transition is apparent in our two simulations at  $\Gamma_{crit}/\Gamma = 1$  by observing the sharpening of the peaks and the emergence of the ‘double peaked’ peaks as opposed to the approximately sinusoidal behavior for the liquid. It is worth noting that only for the lowest  $\Gamma_{crit}/\Gamma$  simulations is  $g(35 \text{ fm}) \approx 0$ , so our calculations of  $Q_6$  using this cut-off includes only on average 14 nucleons for high  $\Gamma_{crit}/\Gamma$  simulations. Nevertheless, this is a small effect which we do not study further.

We can understand the behavior of  $Q_6$  in terms of the temperature and position-space distribution of ions, shown in Fig. 1. For liquids,  $\Gamma_{crit}/\Gamma \geq 1$ , and we expect similar distributions of ions for all temperatures. A slight leftward skew (toward lower  $Q_6$ ) that appears with increasing effective temperature (*i.e.* greater  $\Gamma_{crit}/\Gamma$ ) may be interpreted as the effect of greater average thermal fluctuations. Meanwhile, for solids with  $\Gamma_{crit}/\Gamma \leq 1$ , the reduction in thermal energy suppresses thermal fluctuations on lattice sites, resulting in a sharpening of the distribution of  $Q_6$  as ions converge on an idealized lattice with high local order, as seen in Fig. 1.

With structural characterizations for the OCP complete we move on to study the MCP.

#### B. Multicomponent Plasmas

##### 1. Mixtures

We study six mixtures from Mckinven *et al.* (2016) [23]. That work calculated the phase separation that occurs for rp-ash mixtures in equilibrium that were 50% solid and 50% liquid. In this work we perform molecular dynamics simulations of only the solid component of those mixtures. This differs from past work which was concerned with simulating the phase separation which included both the solid and liquid components (see Caplan *et al.* 3).

These mixtures correspond to the burning products for six different accretion rates of solar composition (helium

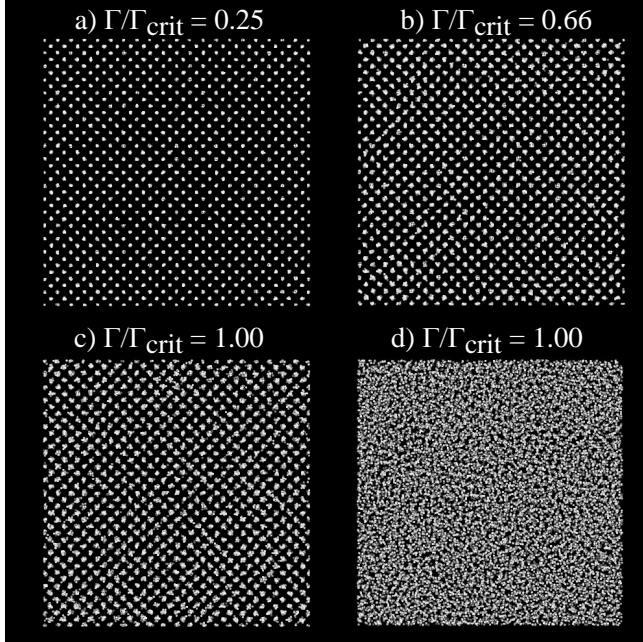


FIG. 1. MD visualizations of an orthographic projection of the bcc (100) plane in an OCP. (a) At the lowest temperatures we find that the lattice has converged to a nearly ideal bcc structure. (b) For greater temperatures, we resolve the thermal fluctuations in the lattice resulting in a smearing of points. (c) At the melting temperature, the thermal fluctuations on lattice sites produce displacements comparable to the lattice spacing, while (d) the melted system at the same temperature demonstrates minimal order.

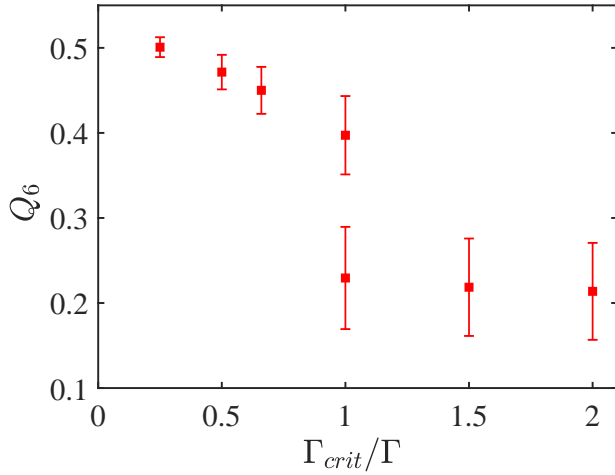


FIG. 3.  $Q_6$  for our OCPs. Points and error bars are mean and standard deviation of  $Q_6$  distributions shown in Fig. 2. We resolve both the sharpening of the distribution for solids with low  $\Gamma_{crit}/\Gamma$  and the approximately constant behavior for liquids with high  $\Gamma_{crit}/\Gamma$ . Compare with the results for the MCP below.

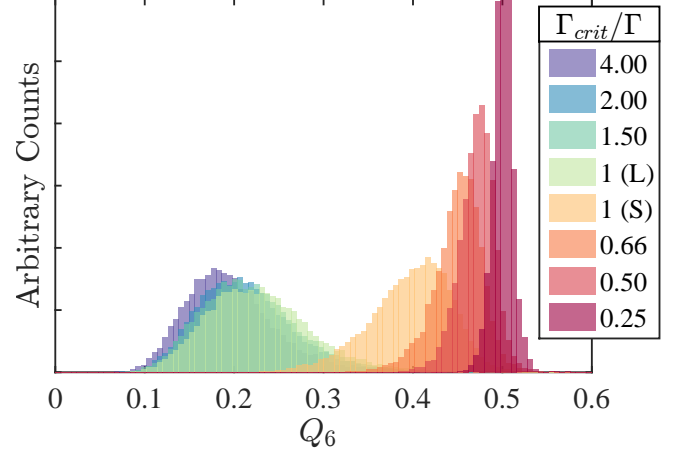


FIG. 2. (Color online) Histograms of ion bond order parameter  $Q_6$  for a set of OCPs. While the liquids all demonstrate a mean  $Q_6 \approx 0.2$ , for solids the  $Q_6$  varies with temperature between approximately 0.4 and 0.5, where the tightening of the distribution is understood as a reduction in thermal fluctuations on the lattice. The two simulations at  $\Gamma_{crit}/\Gamma = 1$  are solid (S) and liquid (L) respectively and run at the melting temperature. A deficit of ions with  $Q_6 \sim 0.3$  suggests that the bond order parameter is useful for discriminating between solid-like and liquid-like ions in pure phases based solely on the arrangement of their neighbors.

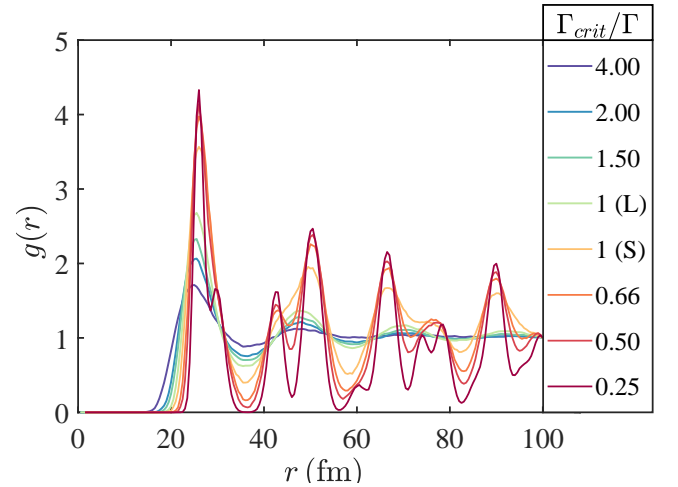


FIG. 4. (Color online) Radial distribution functions  $g(r)$  for the OCP. Color scheme and labeling is the same as Fig. 2. The function broadens smoothly with increasing  $\Gamma_{crit}/\Gamma$  between the known results for a bcc solid and liquid, with the transition at  $\Gamma_{crit}/\Gamma$  being resolved clearly.

TABLE I. Summary of Mixtures

	$\langle Z \rangle$	$Q_{imp}$	$\langle Z^{5/3} \rangle$	$\Gamma_e$	$Z_{max}$	$Z_{min}$	$\Gamma_{max}$	$\Gamma_{min}$	$\Gamma_{MCP}$
Mixture #1	11.2	3.1	57.2	5.841	24	8	1166.3	186.9	333.9
Mixture #2	23.7	7.5	196.6	1.539	26	8	351.1	49.2	302.5
Mixture #3	24.8	4.6	212.5	1.340	28	8	346.1	42.9	284.8
Mixture #4	26.8	8.7	241.1	1.202	30	8	348.3	38.5	289.9
Mixture #5	28.0	8.5	261.7	1.087	32	11	350.5	59.1	284.4
Mixture #6	32.1	27.7	334.4	1.119	44	16	613.5	113.7	374.1

Full list of species and abundances for each mixture are available in the appendix. We report here: mean ion charge  $\langle Z \rangle$ , variance in ion charge  $Q_{imp}$ , mean of ion charge to the 5/3 power  $\langle Z^{5/3} \rangle$  (different from  $\langle Z \rangle^{5/3}$ ), reference  $\Gamma_e$  such that  $\Gamma_i = Z_i^{5/3} \Gamma_e$  (which depends on temperature), the greatest and smallest charges included in the mixture  $Z_{max}$  and  $Z_{min}$  and associated  $\Gamma_i$  for those species. Total mixture  $\Gamma_{MCP} = \langle Z^{5/3} \rangle \Gamma_e$  is effectively the chosen temperature we simulate at.

mass fraction  $Y = 0.2752$ ) material. These accretion rates are  $\dot{m}/\dot{m}_{Edd} = 0.1, 0.2, 0.3, 0.5, 1.0,$  and 10 in units of the Eddington accretion rate  $\dot{m}_{Edd}$ . We refer to these mixtures hereafter as mixtures #1-#6 respectively, and refer to the concentrations (number abundances) of their components with charge  $Z_i$  as  $c_{Z_i}$ . We note that the mixture #2 that we use in this work is different from what is reported in Mckinven *et al.* (*i.e.*  $\dot{m}_{Edd} = 0.2$  in their Tab. 1). That work reports a high impurity parameter for the solid produced by phase separation of the parent mixture, with a large concentration of  $Z = 12$  ions in the solid. Further work on this mixture suggests that it is near a eutectic point, similar to the discussion in Caplan *et al.* 3. We have recalculated the phase separation and find this mixture is depleted in  $Z = 12$  nuclei, producing a much purer solid which is comparable to the other mixtures reported in that work [24].

The phase separation of the parent mixtures that produce these solids are described in some detail in Tab. 1 and Fig. 1 of Mckinven *et al.*, and we include in the appendix a detailed list of the ions and abundances used in our calculations. We exclude species with concentrations less than  $10^{-5}$ . We treat all nuclei of the same charge as having the same mass, chosen as either the mass of the most abundant isotope, or as the average mass of all isotopes rounded to the nearest integer when several isotopes have comparable abundances (*i.e.* we use  $(Z, N+1)$  when pairs of even-even isotopes at  $(Z, N)$  and  $(Z, N+2)$  have comparable abundance). In Tab. III B 1 we summarize some key features of the mixtures. It is worth noting that the  $\Gamma_{MCP}$  reported here is different than  $\Gamma_S$  in Tab. 1 of Mckinven, though one might naively expect these to be the same. The  $\Gamma_S$  reported in that work is specifically the plasma parameter for the solid part of a 50-50 solid-liquid system that is in equilibrium following phase separation of the parent mixture. This is not necessarily the  $\Gamma$  (*i.e.* temperature) the lone solid mixture freezes at, and so our mixture here which excludes the liquid need not be simulated at this specific temperature.

## 2. Simulations

The preparation of these configurations is considerably more detailed than the OCP, as we want to study a realistic crystal which is not heavily biased by initial conditions. To briefly summarize, the simulations are initialized as a liquid with a uniform random distribution and cooled until they freeze to form a crystalline solid. This solid is then equilibrated (*i.e.* allowed to evolve to equilibrium) at constant temperature.

These six simulations all contain 102,400 ions at a density of  $7.18 \times 10^{-5} \text{ fm}^{-3}$ , with a timestep of 25 fm/c, in a cubic volume with periodic boundaries as before. The one exception is the simulation of mixture #1, which includes 204,800 nucleons which also serves as a comparison to check for finite size effects. These simulations are all initialized from random positions and velocities are randomly generated with a Maxwell Boltzmann distribution whose temperature is chosen to be above the temperature given by Mckinven *et al.*, given as  $\Gamma_s$  in that work. This produces liquid configurations which are simulated at constant temperature for at least  $10^6$  MD timesteps ( $2.5 \times 10^7$  fm/c). The simulations are then cooled by rescaling the velocities every 1000 timesteps to a Maxwell-Boltzmann distribution to decrease the temperature by  $5 \times 10^{-6}$  MeV. This cooling is simulated in intervals of  $10^6$  timesteps, which continues until the configuration freezes. The instant of freezing is straightforward to identify as the energy per particle shows a sharp decline consistent with a first order phase transition and the lattice structure becomes visible by inspection, as in Fig. 1. This general equilibration scheme has been used extensively in past work [3, 14, 15].

The simulation configurations generated immediately after the phase transition (*i.e.* the highest temperature we are certain the solid is stable and will not spontaneously melt) is then evolved at constant temperature for  $8 \times 10^8$  timesteps ( $2 \times 10^9$  fm/c) over two simulations of  $4 \times 10^8$  timesteps ( $10^9$  fm/c) each. Over the first simu-

lation the energy is observed to asymptotically decrease, suggesting that the newly formed solid is relaxing to an equilibrium. Over the second simulation we observe that the total energy is constant, suggesting that our six configurations have equilibrated.

As the static structure factor  $S(q)$  has been used extensively in past work it is appropriate to comment here on our choice here to not report  $S(q)$ . This work is considering high lattice temperatures (*i.e.*  $T \lesssim T_{melt}$ ) which are significantly greater than the lattice Debye temperature. This implies that the thermal conductivity is dominated by electron-phonon scattering in the astrophysically relevant regime, as in Deibel *et al.* 25 (see also Potekhin *et al.* 26). Any static structure factors reported in this work would be phonon dominated, rather than impurity dominated. Future work may be interested in studying the  $S(q)$  for the configurations generated in this work quenched to low temperature.

### 3. Crystal Structure

Ions in our simulations crystallize and form a bcc lattice, as in the OCP case. From inspection, the crystals formed in our simulations of mixtures #2, #3, and #5 appear without any immediately apparent structural defects such as dislocations or grain boundaries, while mixtures #1, #4, and #6 may contain dislocations, but are otherwise perfect bcc crystals. This is expected to have only a small effect on the bond order parameters we calculate, as a planar defect in a cubic volume will only involve order  $N^{2/3}$  ions; for simulations with 102,400 ions this effect is of order  $10^{-2}$ .

We find little evidence for continued phase separation which suggests that these mixtures may be stable under the conditions we simulate. We show a subvolume of one configuration generated during the simulation of mixture #3 in Fig. 5. The most abundant ion species in this mixture has  $Z = 26$  with concentration  $c_{26} = 0.427$ . Ions with charges of  $Z = 26$  or greater are shown in white, while ions with decreasing charge are shown with increasing redness. Ions with charge  $Z \leq 22$  have a total concentration of 0.152 and are shown in red. Most of these red points do appear on lattice sites indicating that low  $Z$  impurities are not necessarily interstitial, nevertheless the few interstitial points that are easily identifiable are all low  $Z$  ions. In the upper left region of the figure there is a cluster of interstitial low  $Z$  ions. This is largely due to the projection in the third dimension; many of these points are well separated, though it could be taken to be evidence of clustering of light nuclei and further phase separation, as seen by Horowitz *et al.* 15.

We show  $Q_6$  for select species in these mixtures in Fig. 6. We have separated  $Q_6$  by species in each mixture to show the trend with species charge  $Z$  (identified in the legend). The legends present species in order of decreasing abundances, so that approximate abundances can be seen in the relative heights of the histograms

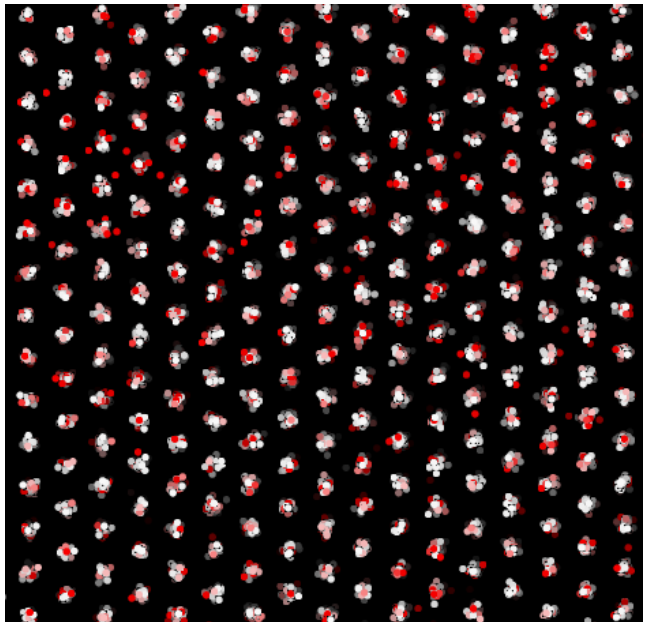


FIG. 5. (Color online) Subvolume of a molecular dynamics simulation of mixture #3. Each point represents one ion. The simulation is fully 3D, though we present an orthographic projection of the bcc (100) face here for clarity. The clustering on lattice sites is due to the distribution of ions in the third dimension. The crystal forms a bcc lattice with a single domain and without any immediately apparent structural defects. Ions with charge near the mixture average and above are shown in white, while those with low charge appear in red. The colors are dimmed with increasing depth in the field, and the red-saturation shows the relative charge. Note that most interstitial ions are red, particularly in top left.

(most abundant in purple, least abundant in red). For readability, some low abundance species have their bin widths rescaled and we omit a number of species from these plots. We choose to show only the most abundant species as well as those which clearly demonstrate the general behavior of low  $Z$  species.

Direct comparisons between mixtures may be difficult as mixtures have different average charge and were simulated at different temperatures. Nevertheless, trends are apparent. In every mixture high  $Z$  ions have a high average  $Q_6$  ( $\approx 0.45$ ), as in the solid OCP, but these distributions now have left skew. Ions with  $Z$  much lower than the mixture average (most visibly  $Z = 12$  in mixture #3 and mixture #5) show broader distributions with lower average  $Q_6$  ( $\approx 0.3$ ). Physically, high  $Z$  ions all have more regularly arranged nearest neighbors. Below some threshold in  $Z$ , ion nearest neighbors become less regular, and low  $Z$  ions are found at centers of local disorder.

In Fig. 7 we present more detailed information about  $Q_6$  for mixture #4. This plots shows representative behavior for all six mixtures. We plot all components of the mixture, resolving more clearly the intermediate behavior of low  $Z$  species. To compare with the OCP in Fig. 3, recall that increasing  $Z_i$  corresponds to an effectively

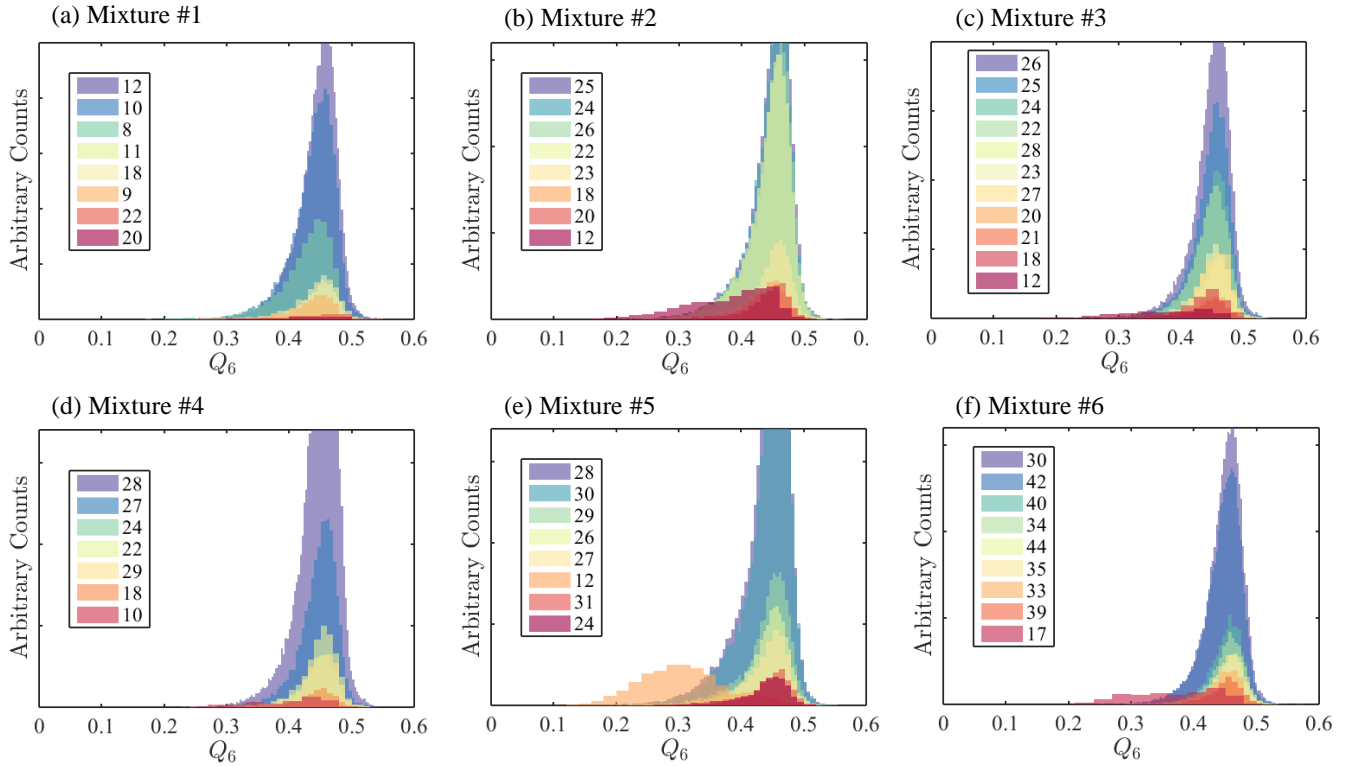


FIG. 6. (Color online) Histograms of ion bond order parameter  $Q_6$  for select ion species in our six MCPs. Legends show ion charge  $Z$ , in decreasing order of abundance. Relative heights of distributions show the relative abundance of ions within a mixture, though some bin widths for the least abundant species have been rescaled for readability. Compared to the OCP, we find a greater left skew in our distributions. Furthermore, the lowest  $Z$  species (*i.e.* those with  $\Gamma_i < 175$ ) in the mixture have much broader distributions with lower average  $Q_6$  relative to the mixture average.

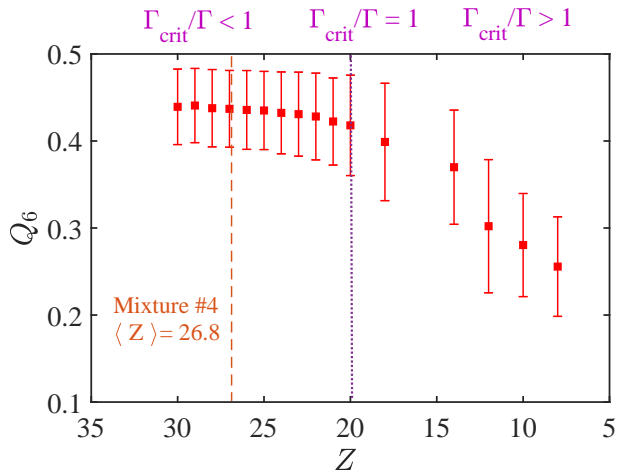


FIG. 7.  $Q_6$  for all species in for mixture #4. Points and error bars are the average and standard deviation of  $Q_6$  for ions of that respective species;  $x$  axis reversed for ease of comparison with Fig. 3. Species near the average mixture charge (dashed line) all show similar solid-like behavior as  $\Gamma_{crit}/\Gamma > 1$ , as in Fig. 6, while ions with  $\Gamma_{crit}/\Gamma < 1$  are increasingly liquid-like  $Q_6$ .

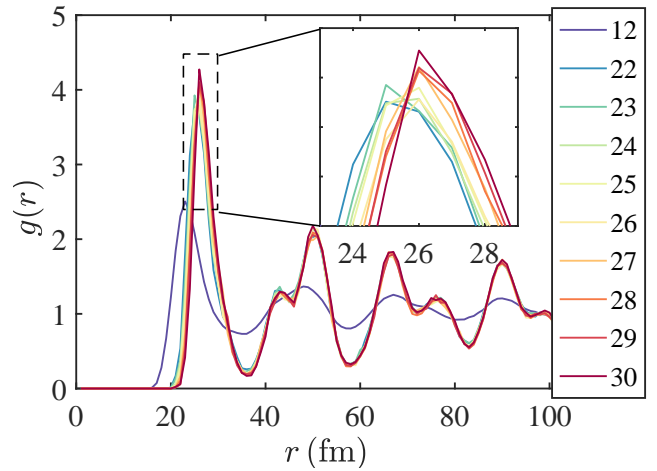


FIG. 8. (Color online) Radial distribution functions  $g(r)$  for mixture #4. Species are shown in order of increasing charge for ease of comparison with the OCP in Fig. 4 ( $\Gamma_{crit}/\Gamma \propto Z_i^{-1}$ ). Observe that the lowest charge plotted ( $Z = 12$ ,  $\Gamma_{crit}/\Gamma = 2.3$ ) shows liquid characteristics, while all other species are consistent the known result for a bcc solid at  $\Gamma_{crit}/\Gamma_{MCP}$ . Inset shows the separation in the first peak with charge, discussed in the text.

decreased  $\Gamma_{crit}/\Gamma_i$ , so that if the MCP were just a linear sum of its component OCPs we would expect the average  $\bar{Q}_6$  to increase asymptotically with  $Z$  to  $\bar{Q}_6 \approx 0.5$ , while the width of its distribution  $\sigma_{Q_6}$  should decrease. In contrast to the OCP, all species for which  $\Gamma_{crit}/\Gamma_i < 1$  show approximately the same behavior, which is approximately that of the mixture average, *i.e.* there is some equivalent  $\Gamma_{OCP}$  which describes high  $Z$  ions in this mixture such that  $\Gamma_{OCP} \approx \Gamma_{MCP}$ . Furthermore, near  $Z = 20$  (*i.e.*  $\Gamma_{crit}/\Gamma_i = 1$ ),  $\bar{Q}_6$  begins smoothly decreasing. This intermediate behavior may be analogous to a glass transition, or indicative of a similar second order phase transition.

In Fig. 8 we show the radial distribution functions  $g(r)$  for mixture #4, again taken to be representative of all our mixtures. These  $g(r)$  are calculated between all ions of species  $j$  and species  $i$  which is taken to be  $Z = 28$ , which comprises more than half of the mixture. Species abundant to less than  $c_j < 4 \times 10^{-3}$  are excluded due to poor statistics. Observe that  $g(r)$  for the lowest charge species in the mixture  $Z = 12$  is the known result for a liquid, while for all other species shown here we see the known result for a bcc solid at finite temperature. This supports our interpretation of Fig. 6 above which argues that low  $Z$  species are in a liquid-like state within the lattice. In the inset, the first peak of  $g(r)$  shows a separation in charge with the first peak shifting to greater  $r$  for greater  $Z$ . However, no such separation is observed for higher order peaks. We argue that this is evidence of screening on the lattice. Lattice spacing is preserved out to large  $r$ , so the lattice remains ordered over a large number of lattice sites. However, the shifting in nearest neighbors may be due to the Coulomb repulsion between individual ions. Lower  $Z$  ions have weaker Coulomb repulsion relative to the lattice, and so they may be closer to high charge neighbors than the average lattice spacing, while high  $Z$  ions have greater Coulomb repulsion and thus will have greater average separation from neighbors. The absence of any separation in the second order peaks or higher suggests that this is a local effect where high  $Z$  ions are screened by low  $Z$  nearest neighbors so that neighboring cells have an average charge close to the mixture average.

#### IV. DISCUSSION

We characterize the structure of the OCP and MCP near the melting temperature using the bond order parameter  $Q_6$  and radial distribution function  $g(r)$ , finding generally that the structure of the MCP is more complicated than a linear sum of the OCP behavior of its components. We interpret the behavior of the majority of species in our mixtures to be that of a solid having crystal properties similar to an OCP with equivalent  $\Gamma_{OCP} = \Gamma_{MCP}$ , *i.e.* the bond order parameter and radial distribution functions are effectively those of the one component plasma at the mixture average temperature

for species where  $\Gamma_{crit}/\Gamma_i < 1$ . Trace low  $Z$  species for which  $\Gamma_{crit}/\Gamma_i > 1$  show intermediate behavior between what was shown for solid and liquid OCPs, including liquid-like radial distributions relative to the lattice average and low average values for the bond order parameter. This ‘quasi-liquid’ behavior suggests that low  $Z$  ions may congregate together in regions with low local order, such as near grain boundaries, dislocations, or in local pockets of liquid embedded within the solid. These sorts of structural defects have been reported for the MCPs simulated by Hughto *et al.* and Caplan *et al.*

We observe screening effects in our simulations of MCPs, with nearest neighbor separations being affected by ion charge but higher order neighbors all being found at the lattice average separation regardless of charge. This screening behavior may be relevant to calculations of the transport properties of the crystal, in particular the thermal and electrical conductivities. Many astrophysical models rely heavily on the impurity parameter  $Q_{imp} = (1/n)\sum_i n_i (\bar{Z} - Z_i)^2$  defined as the variance in mixture charge, which does not contain information about the lattice structure [27]. The impurity parameter formalism was developed assuming a small number of impurities randomly distributed in a relatively pure lattice and may not generalize to mixture with many components of similar abundance. Recent work by Roggero and Reddy 18 finds that, for mixtures similar to those studied in this work, the effective impurity parameter when accounting for lattice effects is a factor of 2-4 lower than would be predicted from  $Q_{imp}$  alone. We explain this physically in terms of the lattice structure. Low  $Z$  and high  $Z$  ‘impurities’ may tend to fall on adjacent lattice sites, screening each other and preserving long range order in the lattice. For accurate calculations of the transport properties of MCPs past work has relied on computationally expensive MD and PIMC simulations. Taken together with the work by Roggero, these calculations may motivate theoretical work to efficiently determine effective transport properties for a given mixture knowing only the composition which do not rely on computationally expensive simulations.

Future work may seek to study how the lattice formed by these mixtures evolves when annealed to lower temperatures. For example, as  $\Gamma_{crit}/\Gamma_i \ll 1$  for all species, the low  $Z$  interstitial defects may either be frozen in or they may migrate to lattice sites, though this will be difficult to study directly with molecular dynamics simulations owing to the long equilibration times and low diffusion rates at low temperatures. Still, such simulations may be interesting and their static structure factors may provide useful insight for improving estimates of the effective impurity parameter in accreting neutron stars.

This work may motivate future studies of structural properties in MCPs, such as diffusion, which is relatively unstudied in the literature. Though this is conjecture, the intermediate behavior in  $Q_6$  observed for low  $Z$  species may generalize to other crystalline properties, such as diffusion coefficients. Following from linear mix-



ing theory, low  $Z$  ions likely have higher mobility within the lattice, having less Coulomb energy relative to the lattice average. Their larger (relative) thermal energies may raise their diffusion coefficients relative to the lattice average, having a greater tunneling probability for lattice site hops. For example, Hughto *et al.* calculated diffusion coefficients for the OCP and found that the diffusion coefficients for a solid at the melting temperature are two orders of magnitude lower than for a liquid. We conjecture that an intermediate diffusion regime exists in MCPs near the melting temperature which may be studied in future work, where low  $Z$  constituents of the solid with  $\Gamma_{crit}/\Gamma_i > 1$  diffuse almost freely within the lattice, but with suppressed diffusion relative to a purely liquid OCP due to the rigid lattice structure. If diffusion rates evolve smoothly near  $\Gamma_{crit}/\Gamma_i = 1$  in mixtures, then there could be a number of implications for astrophysics. Such diffusion rates would be relevant for the evolution of the crystal structure and composition both during freezing and as the mixture evolves to lower effective

temperature (*i.e.* lower  $\Gamma_{crit}/\Gamma_{MCP}$ ), specifically in freezing white dwarfs and accreting neutron stars.

*Acknowledgements:* We thank C. Horowitz, A. Cumming, R. Mckinven, and E. Brown for helpful conversations and the Canadian Institute for Theoretical Astrophysics and the Institute of Nuclear Theory for hospitality. This work benefited from support by the National Science Foundation under Grant No. PHY-1430152 (JINA Center for the Evolution of the Elements). The authors acknowledge the Indiana University Pervasive Technology Institute for providing HPC (Big Red II) and storage resources that have contributed to the research results reported within this paper. This research was supported in part by Lilly Endowment, Inc., through its support for the Indiana University Pervasive Technology Institute, and in part by the Indiana METACyt Initiative. The Indiana METACyt Initiative at IU was also supported in part by Lilly Endowment, Inc. This material is based upon work supported by the National Science Foundation under Grant No. CNS-0521433.

- 
- [1] P.-E. Tremblay, G. Fontaine, N. P. G. Fusillo, B. H. Dunlap, B. T. Gänsicke, M. A. Hollands, J. J. Hermes, T. R. Marsh, E. Cukanovaite, and T. Cunningham, *Nature (London)* **565**, 202 (2019), arXiv:1908.00370 [astro-ph.SR].
- [2] L. Bildsten and D. M. Hall, *The Astrophysical Journal* **549**, L219 (2001).
- [3] M. E. Caplan, A. Cumming, D. K. Berry, C. J. Horowitz, and R. Mckinven, *The Astrophysical Journal* **860**, 148 (2018).
- [4] M. E. Caplan and C. J. Horowitz, *Rev. Mod. Phys.* **89**, 041002 (2017).
- [5] E. F. Brown and A. Cumming, *The Astrophysical Journal* **698**, 1020 (2009).
- [6] O. Vaulina, S. Khrapak, and G. Morfill, *Phys. Rev. E* **66**, 016404 (2002).
- [7] M. Baus and J.-P. Hansen, *Physics Reports* **59**, 1 (1980).
- [8] J. Daligault, *Phys. Rev. Lett.* **108**, 225004 (2012).
- [9] N. R. Shaffer, S. D. Baalrud, and J. Daligault, *Phys. Rev. E* **95**, 013206 (2017).
- [10] A. A. Kozhberov and D. A. Baiko, *Physics of Plasmas* **22**, 092903 (2015).
- [11] C. J. Horowitz, J. Hughto, A. Schneider, and D. K. Berry, “Neutron Star Crust and Molecular Dynamics Simulation,” (Nova Science Publishers, 2012) Chap. 1.
- [12] J. Daligault and S. Gupta, *The Astrophysical Journal* **703**, 994 (2009).
- [13] A. Y. Potekhin, G. Chabrier, and F. J. Rogers, *Phys. Rev. E* **79**, 016411 (2009).
- [14] C. J. Horowitz, D. K. Berry, and E. F. Brown, *Phys. Rev. E* **75**, 066101 (2007).
- [15] C. J. Horowitz, O. L. Caballero, and D. K. Berry, *Phys. Rev. E* **79**, 026103 (2009), arXiv:0804.4409 [astro-ph].
- [16] S. Ogata, H. Iyetomi, S. Ichimaru, and H. M. Van Horn, *Phys. Rev. E* **48**, 1344 (1993).
- [17] N. Itoh and Y. Kohyama, *Astrophys. J.* **404**, 268 (1993).
- [18] A. Roggero and S. Reddy, *Phys. Rev. C* **94**, 015803 (2016).
- [19] W. Lechner and C. Dellago, *J. Chem. Phys.* **129**, 114707 (2008), arXiv:0806.3345 [cond-mat.soft].
- [20] Y. Wang, S. Teitel, and C. Dellago, *J. Chem. Phys.* **122**, 214722 (2005), arXiv:cond-mat/0408458 [cond-mat.mtrl-sci].
- [21] A. L. Thornework, R. Roth, D. G. A. L. Aarts, and R. P. A. Dullens, *The Journal of Chemical Physics* **140**, 161106 (2014), <https://doi.org/10.1063/1.4872365>.
- [22] This ion density is largely irrelevant as  $\Gamma$  is sufficient to fully describe the system, however it does determine the nearest neighbor spacing and gives the first minimum in the bcc radial distribution function at 35 fm.
- [23] R. Mckinven, A. Cumming, Z. Medin, and H. Schatz, *Astrophys. J.* **823**, 117 (2016), arXiv:1603.08644 [astro-ph.SR].
- [24] R. Mckinven, (2019), personal communication.
- [25] A. Deibel, A. Cumming, E. F. Brown, and D. Page, *The Astrophysical Journal* **809**, L31 (2015).
- [26] A. Y. Potekhin, D. A. Baiko, P. Haensel, and D. G. Yakovlev, *Astronomy and Astrophysics* **346**, 345 (1999).
- [27] F. V. de Blasio, “Monthly Notices of the Royal Astronomical Society” **299**, 118 (1998).

## Appendix A: Mixture Tables

TABLE II. Complete list of mixtures studied in this work, with ion charge  $Z$ , ion mass  $A$ , and total number abundance  $N$  and fractional number abundance  $n = N/102400$ . As described in the text, we take all ions of the same charge to have the same mass, though real mixtures will have a range of isotopes.

Mixture # 1				Mixture # 2				Mixture # 3			
$Z$	$A$	$N$	$n$	$Z$	$A$	$N$	$n$	$Z$	$A$	$N$	$n$
12	24	56771	0.55440	25	57	24788	0.24207	26	59	43766	0.42740
10	20	29091	0.28409	24	55	23909	0.23348	25	57	18638	0.18201
8	16	7330	0.07158	26	58	20671	0.20186	24	55	13079	0.12772
11	23	4489	0.04383	22	52	20160	0.19687	22	52	12154	0.11869
18	40	2771	0.02706	23	53	5770	0.05634	28	62	5020	0.04902
9	19	1638	0.01599	18	40	1570	0.01533	23	53	3166	0.03091
22	52	122	0.00119	20	48	1362	0.01330	27	63	3159	0.03084
20	48	63	0.00061	12	26	1348	0.01316	20	48	1076	0.01050
14	30	38	0.00037	21	49	1218	0.01189	21	49	839	0.00819
21	49	33	0.00032	8	16	678	0.00662	18	40	767	0.00749
24	56	24	0.00023	10	21	349	0.00340	12	25	356	0.00347
23	53	19	0.00018	11	25	327	0.00319	8	16	247	0.00241
17	37	11	0.00010	28	62	190	0.00185	10	21	81	0.00079
				17	38	37	0.00036	11	25	52	0.00050
				14	31	16	0.00015				
				15	34	7	0.00007				

Mixture # 4				Mixture # 5				Mixture # 6			
$Z$	$A$	$N$	$n$	$Z$	$A$	$N$	$n$	$Z$	$A$	$N$	$n$
28	65	60679	0.59256	28	65	37991	0.37100	30	69	32165	0.31411
26	60	14103	0.13772	30	70	34071	0.33272	28	64	27842	0.27189
27	63	9579	0.09354	29	69	11097	0.10836	42	100	8896	0.08687
25	57	4088	0.03992	26	60	8322	0.08126	32	76	5652	0.05519
24	55	3394	0.03314	27	63	3188	0.03113	40	96	5418	0.05291
30	68	2906	0.02837	12	24	2060	0.02011	38	90	4606	0.04498
22	52	2770	0.02705	31	73	1461	0.01426	34	80	4140	0.04042
12	24	2215	0.02163	24	56	1308	0.01277	36	84	3406	0.03326
29	69	726	0.00708	25	57	1057	0.01032	44	103	2602	0.02541
23	53	724	0.00707	22	52	756	0.00738	41	99	1681	0.01641
20	48	369	0.00360	32	74	426	0.00416	35	85	1388	0.01355
18	40	240	0.00234	23	53	189	0.00184	26	60	1296	0.01265
21	49	208	0.00203	14	28	171	0.00166	33	81	1088	0.01062
10	20	188	0.00183	20	48	136	0.00132	31	73	850	0.00830
8	16	172	0.00167	11	25	87	0.00084	39	93	714	0.00697
14	30	39	0.00038	18	40	80	0.00078	16	36	499	0.00487
								17	39	157	0.00153